Hindawi
Adsorption Science & Technology
Volume 2021, Article ID 2359110, 15 pages
https://doi.org/10.1155/2021/2359110

Research Article

Effective Removal of Malachite Green from Aqueous Solutions Using Magnetic Nanocomposite: Synthesis, Characterization, and Equilibrium Study

Ali Q. Alorabi

Chemistry Department, Faculty of Science, Albaha University, P.O. Box 1988, Al Baha 65779, Saudi Arabia

Correspondence should be addressed to Ali Q. Alorabi; aalorabi@bu.edu.sa

Received 30 June 2021; Revised 11 August 2021; Accepted 21 August 2021; Published 15 September 2021

Academic Editor: George Kyzas

In this work, magnetized activated *Juniperus procera* leaves (Fe_3O_4@AJPL) were successfully prepared via chemical activation of JPL and in situ coprecipitation with Fe_3O_4. A Fe_3O_4@AJPL nanocomposite was successfully applied for the elimination of malachite green (MG) dye from aqueous media. The prepared Fe_3O_4@AJPL adsorbent was characterized by SEM, EDX, TEM, XRD, FTIR, TGA, and BET surface area analyses. The BET surface area and pore size of the Fe_3O_4@AJPL nanocomposite were found to be 38.44 m^2/g and 10.6 nm, respectively. The XRD and FTIR results indicated the formation of a Fe_3O_4@AJPL nanocomposite. Different parameters, such as pH of the solution (3–8), adsorbent dosage (10–100 mg), temperature (25–45°C), contact time (5-240 min), and initial MG concentrations (20–350 mg/L), for the elimination of the MG dye using Fe_3O_4@AJPL were optimized and found to be 7, 50 mg, 45°C, 120 min, and 150 mg/L, respectively. The nonlinear isotherm and kinetic studies exhibited a better fitting to second-order kinetic and Langmuir isotherm models, with a maximum monolayer adsorption capacity of 318.3 mg/g at 45°C, which was highly superior to the previously reported magnetic nanocomposite adsorbents. EDX analyses confirmed the presence of nitrogen on the Fe_3O_4@AJPL surface after MG adsorption. The calculated thermodynamic factors indicated endothermic and spontaneous processes. The desorption of MG dye from Fe_3O_4@AJPL was performed using a solution of 90% ethanol. Finally, it could be concluded that the designed Fe_3O_4@AJPL magnetic nanocomposite will be a cost-effective and promising adsorbent for the elimination of MG from aqueous media.

1. Introduction

Water pollution by organic wastes produced by human activities is considered as one of the most dangerous environmental problems which have threatened human health and other living organisms. Dyes are widely utilized in different industries such as pharmaceuticals, paper, plastics, leather, and textiles. Malachite green (MG) has been extensively used in various fields such as in food processing, textile, cosmetic, pharmaceutical, plastic, and paper industries [1]. MG is used in aquaculture industries due to its great fungicide and bactericidal efficacy. Thus, it is extremely toxic to humans, plants, and aquatic fauna [2, 3], and it can cause carcinogenesis damage to the kidney and liver [4, 5]. Due to the toxicity and carcinogenic effect of MG dye ions, their removal from the aqueous environment is highly demanded. Therefore, the removal of dyes such as MG from wastewaters or surface waters is mandatory for the protection of human health. Different techniques were developed by researchers for the dye removal from the wastewater including membrane [6], photodegradation [7, 8], oxidation [9], electrochemical [10] ion exchange [11], and adsorption methods [12–14]. Among these techniques, adsorption is a successful, effective, and economical technique that is used to eliminate dyes from the polluted water as compared to other techniques [15, 16].

Many adsorbent materials were obtained from natural materials such as chitosan [17] and alginate beads [18]; wastes of agricultural activities, for example, almond shell [19], garlic peel [20], coffee waste [21], sugarcane bagasse

[22], orange peels [23], banana peels [24], and peanut hull; and industrial waste, i.e., fly ash [25] for the elimination of dyes from aqueous media. Among the tested natural materials, leaf-based materials have received great attention as they possess various characteristics such as their low cost, easy preparation, and availability in large quantities. Leaves are used as an adsorbent material for the elimination of MG dye from wastewater by reducing the amount of waste produced [26]. Gupta et al. [27] have prepared Ashoka (*Saraca asoca*) leaf powder and tested for the elimination of brilliant green (BG), malachite green (MG), rhodamine B (RB), and methylene blue (MB) from an aqueous solution with 125, 83.3, 66.6, and 90.9 mg/g, respectively, as the maximum adsorption capacity. The treatment of the raw leaf-based material with different chemical reagents such as acids and bases could improve their adsorption properties toward the removal of dyes [28, 29].

Recently, it has been reported that biosorbent treated with H_2O_2 improved the capacity of dye adsorption from the solution since the H_2O_2 could increase oxygen-containing functional groups on the surface of the adsorbent and thus augment its capability to remove dyes from aqueous media [30, 31]. As we know, nonmagnetic material adsorbents suffer from the difficulty of isolation of adsorbate-loaded absorbents from aqueous media after the adsorption process due to their small particle size. To overcome this problem, the use of magnetism has been proposed by several researchers. Magnetite nanoparticles (Fe_3O_4) attract significant attention due to their unique large surface area, and these possess high saturation magnetization and can easily isolate toxic pollutants from aqueous solutions by using a magnet without using centrifugation and filtration compared to conventional adsorbents [32]. New economical, highly effective, and locally available biosorbents are still under development. *Juniperus procera* leaves are the most abundant plant in Saudi Arabia and many countries such as Lebanon, Bosnia, and Turkey [33–36]. Magnetic modification of low-cost adsorbents such as *Juniperus procera* leaves (JPL) could lead to materials appropriate for environmental applications. After a thorough literature survey, we have concluded that there are no previous studies reporting the activation of *Juniperus procera* leaves with H_2O_2 to increase the oxygen-containing functional groups on its surface. To our best knowledge, this is the first work to report the synthesis of a Fe_3O_4@activated *Juniperus procera* leaf nanocomposite.

This study was aimed at synthesizing a new Fe_3O_4@activated *Juniperus procera* leaf nanocomposite (Fe_3O_4@AJPL) via chemical activation and in situ coprecipitation methods. The prepared adsorbent was applied for removal of dyes from aqueous media. The Fe_3O_4@AJPL adsorbent was characterized by SEM, EDX, TEM, XRD, TGA, FTIR, and BET surface area analysis. The impact of various parameters on the MG dye adsorption onto Fe_3O_4@AJPL adsorbent such as solution pH, adsorbent dosage, contact time, initial MG concentrations, and temperature was achieved. The isotherm and kinetic data were analyzed by applying nonlinear equation models. Thermodynamic factors were also calculated.

2. Experiments

2.1. Chemicals and Instrumentation. Malachite green (MG), hydrogen peroxide (H_2O_2, 30%), ferric chloride ($FeCl_3{\cdot}6H_2O$, 97%), ethanol (C_2H_5OH, 99.8%), and ferrous chloride ($FeCl_2{\cdot}4H_2O$, 98%) were procured from Sigma Aldrich. Nitric acid (HNO_3, 68.0-70.0%), sodium hydroxide (NaOH, ≥97%), and hydrochloric acid (HCl, 36%) were procured from BDH, England. Solutions were prepared using deionized water. The crystalline structures of *AJPL*, Fe_3O_4, and Fe_3O_4@AJPL were determined using an XRD-6000 (Shimadzu, Kyoto, Japan). The morphological properties of *AJPL*, Fe_3O_4, Fe_3O_4@AJPL, and Fe_3O_4@AJPL-MG were evaluated using a transmission electron microscope (TEM) and scanning electron microscope (SEM) (JEOL 200 kV, Tokyo, Japan). Fourier transform infrared spectra of activated *Juniperus procera* leaves (*AJPL*), Fe_3O_4@AJPL, and MG-saturated Fe_3O_4@AJPL (Fe_3O_4@AJPL-MG) were recorded using a Nicolet iS50, Thermo Scientific (Madison, WI, USA). The elemental composition of adsorbents was detected by energy-dispersive X-ray (EDX) (JEOL 7600F, Tokyo, Japan). The surface area of Fe_3O_4@AJPL was evaluated through the determination of N_2 adsorption-desorption isotherms at −196°C by Micromeritics (USA). The concentration of MG was determined using a UV-visible spectrophotometer (Shimadzu 2450) at 616 nm.

2.2. Chemical Treatment of Juniperus procera Leaves. *Juniperus procera* leaves (JPL) were collected from Al Baha Province, Saudi Arabia. The leaves were washed with distilled water and dried for 7 days at room temperature (22–27°C) and ground using an electrical grinder. To increase oxygen-containing functional groups on the JPL surface, the JPL was treated with H_2O_2 by using the reported methods [30, 31]. Briefly, 20 g of the obtained JPL powder was immersed in 200 mL of 10% H_2O_2 and stirred for 24 h. Then, the sample was filtered off and was washed several times with deionized water. Following, 20 g of the *AJPL* powder was added into 200 mL of 1 M NaOH for removal of the impurities from the surface of *JPL* powder, resulting in improvement of the surface roughness of particles, formation of a pore structure, and opening of more hydroxyl groups and other reactive functional groups on its surface. Therefore, the removal of surface impurities can improve the adsorption properties of the *JPL* powder [37, 38]. The *JPL* powder was stirred for 24 h at 25°C. The resulting *AJPL* powder was washed with D.I. water and dried at 25°C for 3 days. Finally, the *AJPL*-obtained material was ground again to obtain a uniform particle size (Figure 1).

2.3. Magnetization of Juniperus procera Leaves (Fe_3O_4@AJPL). The magnetization of *AJPL* powder was performed using the in situ coprecipitation method. Briefly, in a three-necked round bottom flask containing 90 mL D.I. water, 1.5 g of AJPL powder was suspended. To this mixture, 0.715 g of $FeCl_2{\cdot}4H_2O$, and 2.15 g of $FeCl_3{\cdot}6H_2O$ (Fe^{2+} : Fe^{3+}=1 : 2 molar ratio) were added and mechanically stirred for 20 min and heated to 80°C, and then, 10 mL of NH_4OH was added dropwise over a period of 2 hrs. The obtained

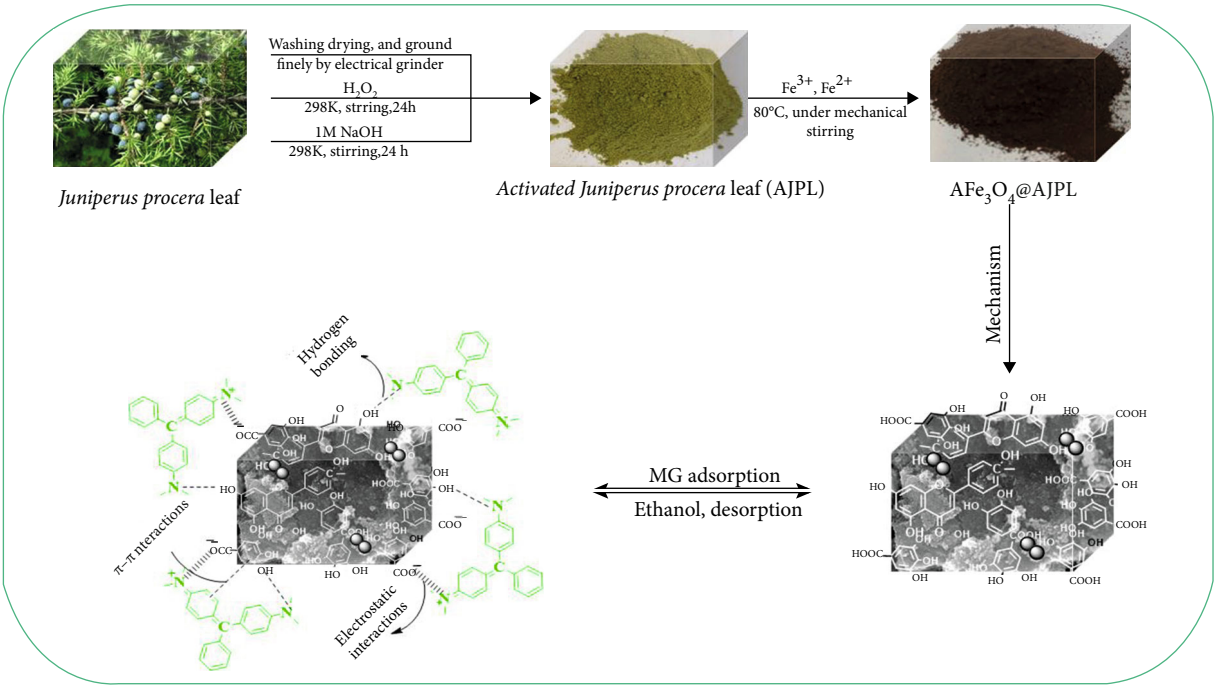

Figure 1: Synthesis of Fe_3O_4@AJPL nanocomposite and its mechanism of adsorption-desorption behavior for MG dye ions.

black precipitate (termed Fe_3O_4@AJPL) was collected by external magnetic field and washed with ethanol and D.I. water. Finally, the Fe_3O_4@AJPL was dried at 60°C for 24 h. Figure 1 demonstrates the preparation scheme of the Fe_3O_4@AJPL nanocomposite.

2.4. Adsorption Studies. The batch experiment method was conducted to select the best parameters for the adsorption process. The impact of adsorption parameters on MG dye adsorption by Fe_3O_4@AJPL adsorbents including adsorbent dosage (10–100 mg), pH (3–8), temperature (25–45°C), contact time (5-240 min), and initial MG dye concentration (20–350 mg/L) was achieved. The general procedure was as follows: the desired quantity of Fe_3O_4@AJPL adsorbents was taken in a 250 mL Erlenmeyer flask containing a 50 mL solution of MG with a given concentration, and then, the sample solution pH was adjusted using a 0.1 M HCl or 0.1 M NaOH to the desired pH. Then, the sample solution was shaken at 100 rpm for a specific time. After that, the sample was separated using a magnet, and the residual MG concentration was measured using a UV/Vis spectrophotometer at 616 nm. The adsorption efficiency (R_e, %) and adsorbent capacity (q_e, mg/g) were determined according to the following equations, respectively:

$$R_e\,(\%) = \frac{C_o - C_e}{C_o} \times 100, \tag{1}$$

$$q_e = (C_o - C_e)\frac{V}{m}, \tag{2}$$

where C_o (mg/L) and C_e (mg/L) represent the initial and equilibrium concentrations of MG, respectively; m is the amount of Fe_3O_4@AJPL adsorbents (g); and V (L) is the solution volume. For the desorption study, the separated adsorbent was placed into 50 mL of 90% ethanol or HCl (0.1 M) and HNO_3 (0.1 M) solution. Then, the sample solution was shaken at 100 rpm for 120 min. After that, the MG dye concentrations of the sample isolated with a magnet were determined using a UV/Vis spectrophotometer at 616 nm. The % desorption was calculated by using the following equation:

$$\%\text{desorption} = \frac{\text{Concentration of MG desorbed by the ethanol}}{\text{Initial concentration of MG adsorbed on } Fe_3O_4\text{@AJPL}} \times 100. \tag{3}$$

3. Results and Discussion

3.1. Synthesis and Characterization of Fe_3O_4@AJPL. *Juniperus procera* leaves (JPL) were activated by using H_2O_2 and NaOH reagent. H_2O_2 is a strong oxidant, inexpensive, and clean. The use of H_2O_2 and NaOH is important to increase oxygen-containing functional groups on the JPL surface and improve the adsorption properties of JPL powder by removing the impurities from the surface of the JPL powder. AJPL carries hydroxyl, carboxyl, and carbonyl groups. Activated *Juniperus procera* leaves were successfully converted to the magnetized activated *Juniperus procera* leaves (Fe_3O_4@AJPL) via in situ coprecipitation. Fe_3O_4@AJPL has the ability to separate MG dye from aqueous solutions by using an external magnetic field, and it has a large surface area (116.9517 m^2/g) and pore size (9.48 nm). It can easily separate the MG dye from aqueous solutions by using an external magnetic field. The Fe_3O_4@AJPL nanocomposite contains different functional groups (COOH,

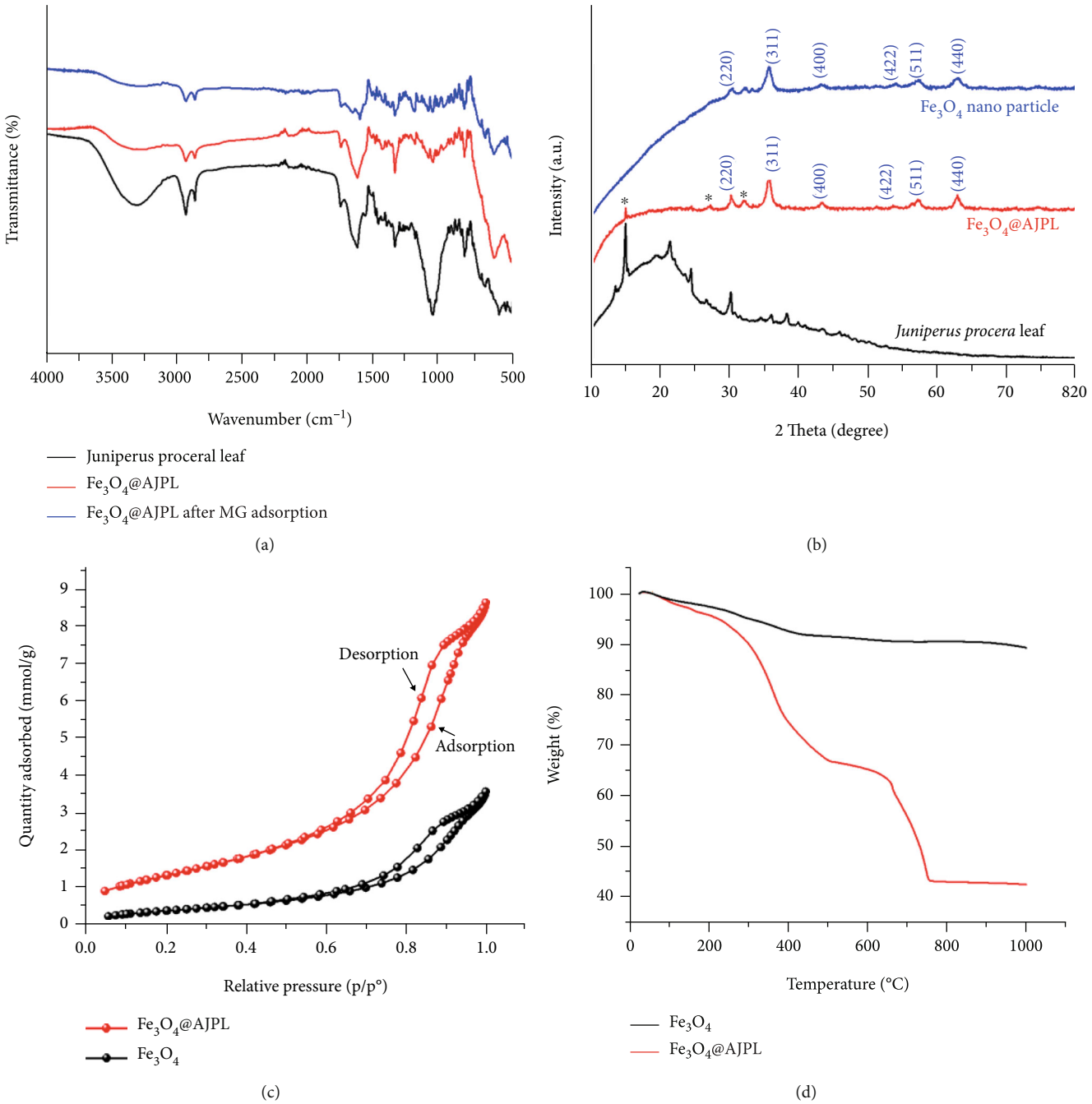

Figure 2: (a) FT-IR spectra, (b) XRD plot, (c) BET adsorption-desorption analysis, and (d) TGA analysis of adsorbents.

OH, C=O) which can adsorb MG ions by for π-π stacking, H-bonding, and electrostatic attraction (Figure 1).

Figure 2(a) displays the FTIR of *AJPL*, Fe_3O_4@AJPL before adsorption, and MG-saturated Fe_3O_4@AJPL (Fe_3O_4@AJPL-MG) adsorbent. In the spectrum of *AJPL*, the broad band centered at 3320 cm^{-1} is attributed to the OH group, suggesting the presence of a phenolic group [39]. The bands at 1731 and 1606 cm^{-1} ascribed to C=O and the one at 1026 cm^{-1} corresponding to C-O-C groups indicate the existence of carboxylic acid derivatives. Furthermore, the observed band of C=C stretching vibration at 1549 cm^{-1} as well as the C-H out-of-plane bending vibrations at 776 cm^{-1} is possibly characterizing the aromatic rings. Additional peaks of CH modes were also identified, e.g., at about 2943 cm^{-1}. In the spectrum of Fe_3O_4@AJPL, a new band at 560 cm^{-1} assigned to the distinctive band of Fe-O stretching vibration was observed, confirming the presence of Fe_3O_4 nanoparticles [40, 41]. Moreover, it is observed that the modification of *AJPL* with Fe_3O_4 nanoparticles has resulted in intensity reduction of some characteristic peaks including the OH and C-O-C peaks. The spectra of the MG-loaded Fe_3O_4@AJPL showed shifts in the bands of

some functional groups such as C=O, OH, and C-O-C from 1731, 3320, and 1026 cm^{-1} to 1721, 3329, and 1023 cm^{-1}, respectively, due to adsorptive interaction.

Figure 2(b) shows the XRD pattern of AJPL, Fe_3O_4 nanoparticles, and Fe_3O_4@AJPL nanocomposite. As implied in Figure 2(b), the characteristic peaks of Fe_3O_4 nanoparticles and the Fe_3O_4@AJPL nanocomposite perfectly matched the face-centered cubic crystalline which was confirmed by 2θ values of 30.24°, 35.56°, 43.22°, 57.11°, and 62.76° to (220), (311), (400), (511), and (440) planes, respectively [42]. The diffraction peaks for AJPL are 13.45°, 14.83°, 21.2°, 24.29°, 30.02°, 35.8°, and 38.15°. After modification of magnetite nanoparticles with AJPL, new peaks appeared at $2\theta = 14.9°$ and 27.02° which matched to the strong peaks in the XRD pattern of leaves [43]. Therefore, these results indicated that the Fe_3O_4@AJPL nanocomposite was successfully synthesized.

Figure 2(c) displays the N_2 adsorption/desorption isotherms of Fe_3O_4 nanoparticles and the Fe_3O_4@AJPL nanocomposite. The surface area, pore volume, and pore size were found to be 116.9517 m^2/g, 0.322 cm^3/g, and 9.48 nm for Fe_3O_4 nanoparticles and 38.44 m^2/g, 0.136 cm^3/g, and 10.6 nm for the Fe_3O_4@AJPL nanocomposite. The N_2 adsorption-desorption curve of both adsorbents exhibited a type IV isotherm, suggesting the presence of mesopores in both adsorbents.

Figure 2(d) shows thermogravimetric analysis (TGA) of Fe_3O_4 and Fe_3O_4@AJPL. In the case of Fe_3O_4, about 10% is the total weight loss in the temperature range from 25°C to 1000°C due to the removal of the adsorbed water and conversion of hydroxide to oxide [44]. In the case of the Fe_3O_4@AJPL nanocomposite, it is a three-stage thermal degradation. The first stage from 25–180°C (3%) is related to the loss of moisture and adsorbed water. 7% and 50% weight loss were observed between the temperature ranges 180–320°C and 320–800°C in the second and third stages, respectively, due to decomposition of molecular organic compounds such as flavonoids of JPL in Fe_3O_4@AJPL [45]. The total weight losses of Fe_3O_4@AJPL and pure magnetite nanoparticles were 60% and 10%, respectively, which confirmed the formation of the Fe_3O_4@AJPL nanocomposite.

Figure 3 shows the SEM-EDX image results of the *AJPL* powder, Fe_3O_4, Fe_3O_4@AJPL, and MG dye-saturated Fe_3O_4@AJPL adsorbents. The surface structure of the *AJPL* powder is rough with the existence of some pore and crack sites (Figure 3(a)). After modifying the *AJPL* powder with magnetite nanoparticles, the magnetite nanoparticles are dispersed in the surface of AJPL (Figure 3(c)). The surface of Fe_3O_4 nanoparticles shows a spherical shape with diameters in the range of 12–25 nm (Figure 3(e)). The SEM image of the Fe_3O_4@AJPL loading MG showed a different morphology than before adsorption, which was well occupied with the MG dye as implied in Figure 3(g), indicating that the MG dye was successfully adsorbed on the Fe_3O_4@AJPL adsorbent. The EDX of the *AJPL* powder (Figure 3(b)) revealed the presence of mainly C (30.68%) and O (30.50%) and small amounts of Ca, Al, K, and Si. After modifying *AJPL* with magnetite nanoparticles, it was clearly observed that a new peak from iron (45.33%) appeared and increased in the intensity of oxygen (38.27%), confirming the synthesis of Fe_3O_4@AJPL successfully (Figure 3(d)). 65.32% of iron and 34.68% of oxygen were observed in the EDX spectrum of pure magnetite nanoparticles (Figure 3(e)). After MG dye was saturated on the Fe_3O_4@AJPL nanocomposite, a new peak of nitrogen was observed, indicating the successful adsorption of MG dye on the Fe_3O_4@AJPL adsorbent Figure 3(h). Figure 4(a) displays the TEM images of Fe_3O_4@AJPL nanocomposite. A small degree of agglomeration with a spherical shape was observed. The particle size was found to be 9 nm Figure 4(b). Figure 4(c) displays the lattice fringe spacing of the crystalline part (Fe_3O_4) of the Fe_3O_4@AJPL nanocomposite. The d spacing values were 0.291 nm and 0.252 nm, which are attributed to the (311) and (220) planes of Fe_3O_4 nanoparticles which were confirmed by the XRD results for the cubic structure of Fe_3O_4 nanoparticles. The selected area electron diffraction (SAED) analysis shows a ring pattern which confirms the presence of crystalline Fe_3O_4 nanoparticles in the nanocomposites (Fe_3O_4@AJPL) (Figure 4(c)).

3.2. Adsorption Studies

3.2.1. Adsorbate Selectivity. The prepared adsorbents *AJPL* and Fe_3O_4@AJPL nanocomposite were examined for elimination of different cationic dyes such as MG, CV, and MB from aqueous solutions as implied in Table 1. It was noticed that, at the adsorption conditions of adsorbent dose 50 mg, initial adsorbate concentration (C_o) of 50 mg/L, and temperature of 25 C, the maximum removal efficiency of MG, CV, and MB dyes on both AJPL and Fe_3O_4@AJPL nanocomposite adsorbent were 98.76%, 94.81%, and 93.20% and 99.15%, 95.61%, and 73.11%, respectively. Accordingly, the removal of MG by the Fe_3O_4@AJPL adsorbent is considerably favored due to the high performance, easy separation, and recovery of the adsorbent using external magnetism. Thus, the adsorption parameters were further studied.

3.2.2. Effect of pH. The impact of the solution pH on MG adsorption onto Fe_3O_4@AJPL was tested over a range of pH values from 3 to 8 (MG: 20 mg/L, contact time: 24 h, adsorbent dose: 50 mg, temperature: 25°C, and agitation: 100 rpm) as shown in Figure 5(a). The results indicate an increase in the adsorption capacity and removal percentage with increase in pH up to pH 7. This increase in adsorption capacity was due to the surface charge of Fe_3O_4@AJPL nanocomposites becoming more negative and having strong electrostatic attraction with the cationic MG dye, resulting in higher adsorption efficiency. On the contrary, under an acidic medium, the excessive protonation of the Fe_3O_4@AJPL nanocomposite surface hindered the binding of cationic MG ions on the Fe_3O_4@AJPL nanocomposite surface, resulting in a lower adsorption efficiency [46]. Similar trends have been reported by Asfaram et al. for the removal of MG using biosorbent *Yarrowia lipolytica* ISF7 [47]. Compared with pH 7, an almost similar performance was observed at pH 8 above which the solution becomes colorless due to the reaction occurrence between the MG and

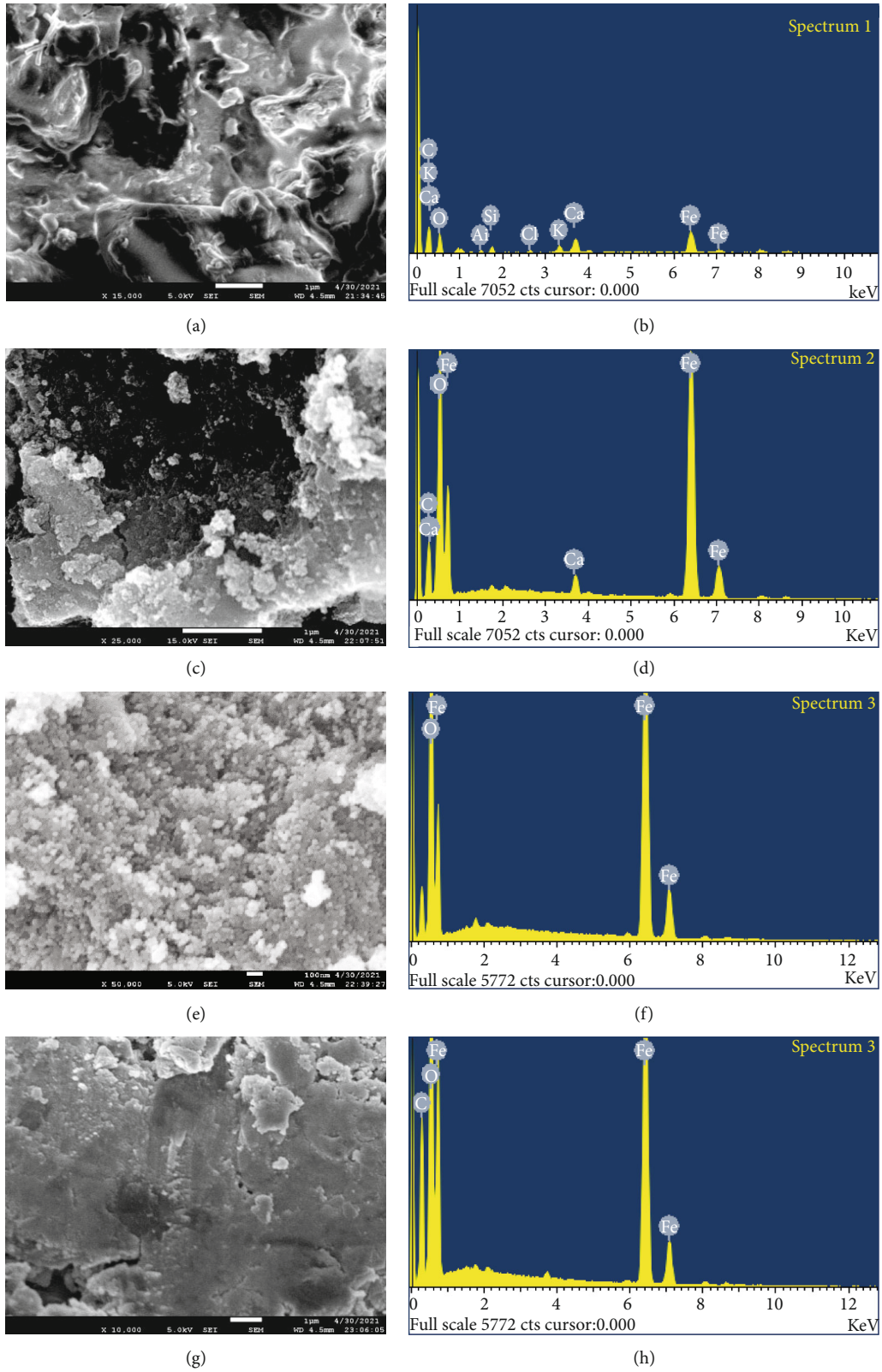

Figure 3: (a) SEM image, (b) EDX analysis of *activated Juniperus procera* leaves (AJPL), (c) SEM image, (d) EDX analysis of Fe_3O_4@AJPL, (e) SEM images, (f) EDX analysis of magnetite nanoparticles, (g) SEM image, and (h) EDX analysis of MG adsorption onto Fe_3O_4@AJPL.

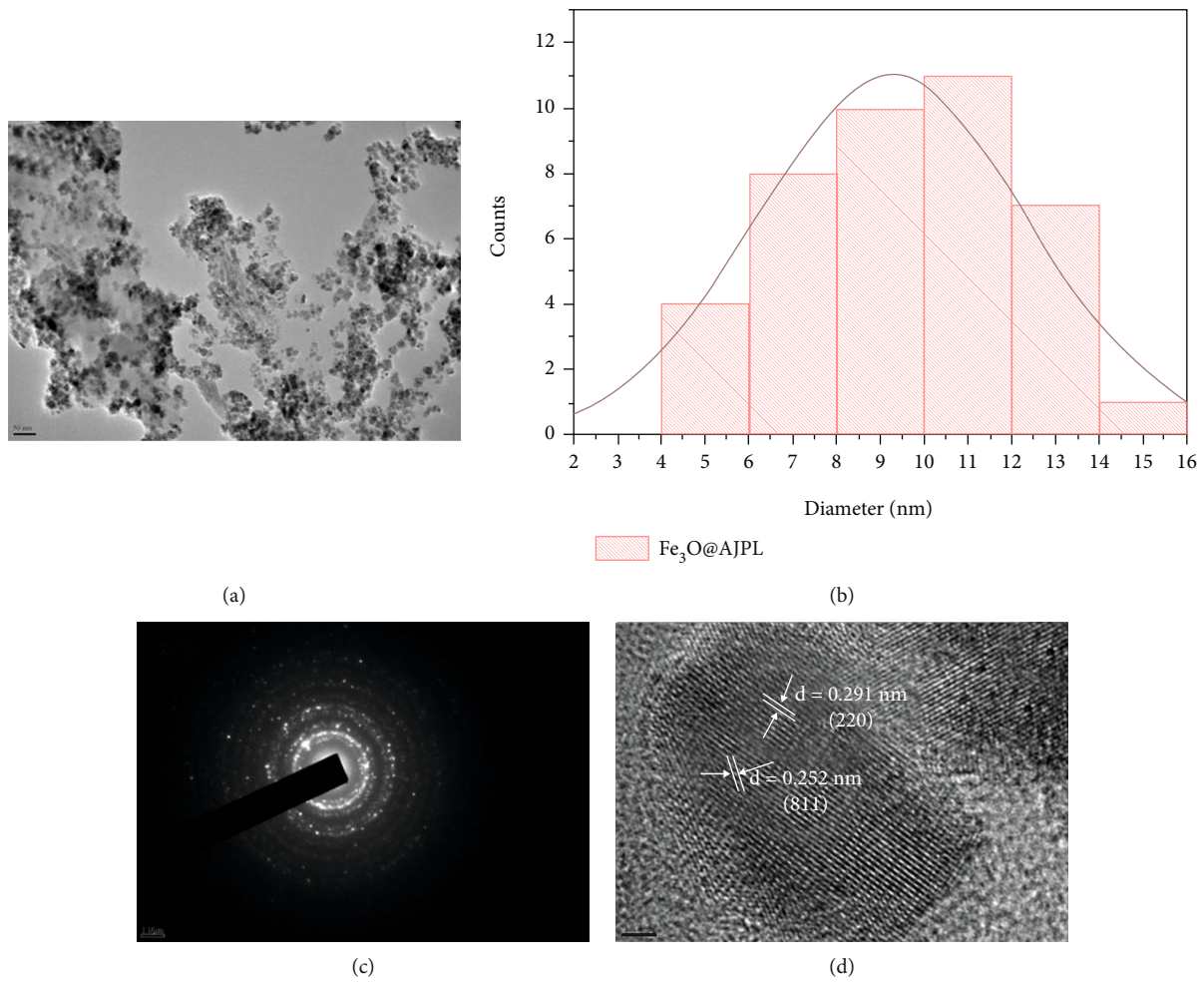

Figure 4: (a) TEM image, (b) size particles distribution, (c) SAED pattern, and (d) HRTEM image of Fe_3O_4@AJPAL adsorbent.

Table 1: Adsorption selectivity experiments with dye solutions (conditions: dye—20 mg/L, time—24 h, Fe_3O_4@AJPAL—50 mg, volume—0.05 L, temperature—25°C, and agitation—100 rpm).

Adsorbents	MG		CV		MB	
	Adsorption capacity (mg/g)	Removal efficiency (%)	Adsorption capacity (mg/g)	Removal efficiency (%)	Adsorption capacity (mg/g)	Removal efficiency (%)
Activated *Juniperus procera* leaves (AJPL)	19.75	98.76	18.96	94.81	18.64	93.20
Fe_3O_4@AJPL	19.83	99.15	19.12	95.61	14.62	73.11

OH. These results are inconsistent with the ones reported by Pan et al. [48] and De Marco et al. [49].

3.2.3. Effect of Contact Time. The impact of the contact time on the MG adsorption by Fe_3O_4@AJPL was achieved over the time interval of 5–240 min under fixed conditions (MG: 20 mg/L, pH: 7, temperature: 25°C dose: 50 mg, and agitation: 100 rpm) (Figure 5(b)). At an initial period of 15 min, the adsorption rate was high with R_e (%) and q_e values of 85.7% and 17.14 mg/g, respectively. The initial rapid rate may indicate the existence of available active sites on the Fe_3O_4@AJPL surface. After 15 min, the adsorption was gradually increased with time, reaching the equilibrium, after 120 min, at which the q_e and R_e (%) were 18.32 mg/g and 91.6% at 120 min, respectively. Thus, the optimized equilibrium time for the work was 120 min. Compared with the literature, this equilibrium time is better than the ones previously reported by Pan et al. [48] and Gao et al. [50].

3.2.4. Effect of Dosage. The impact of the adsorbent dosage on the removal efficiency and adsorption capacity was tested in the range 10-100 mg under the following conditions: MG: 20 mg/L, pH: 7, contact time: 120 min, agitation: 100 rpm, and temperature: 25°C. As shown in Figure 5(c), the R_e (%) value was slightly improved from 94.3% to 99.1% with the gradual rise in the amount of Fe_3O_4@AJPL adsorbent from 10 to 50 mg; however, the capacity (q_e) was reduced. These results can be assigned to increased active sites at a

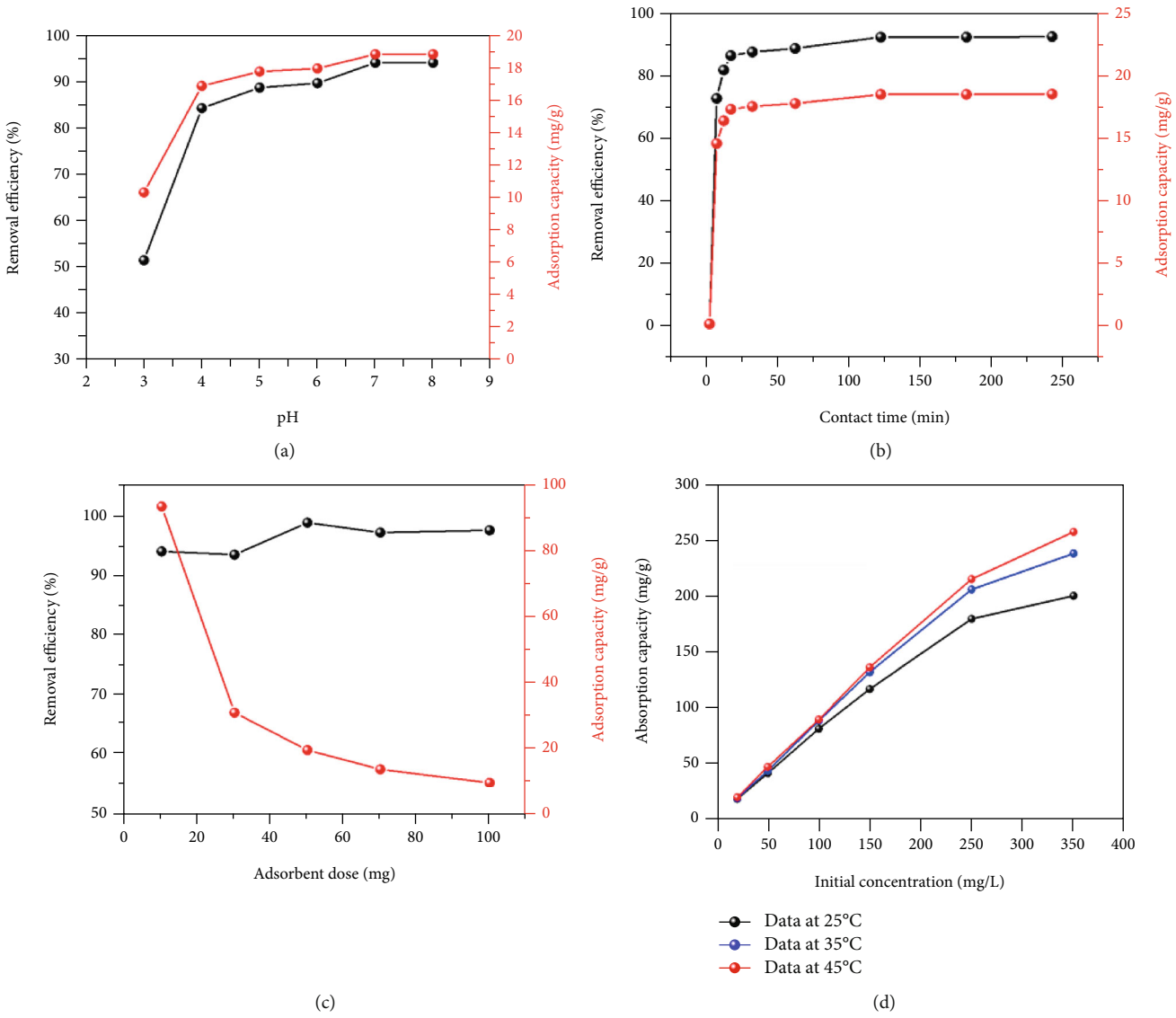

Figure 5: (a) Effect of pH value (conditions: MG—20 mg/L, time—24 h, Fe_3O_4@AJPAL—50 mg, temperature—25°C, and agitation—100 rpm), (b) contact time (conditions: MG—20 mg/L, pH—7, Fe_3O_4@AJPAL—50 mg, agitation—100 rpm, and temperature—25°C), (c) adsorbent dose (conditions: MG—20 mg/L, pH—7, time—120 min, temperature—25°C, and agitation—100 rpm), and (d) initial MG concentration (conditions: time—120, Fe_3O_4@AJPAL—50 mg, pH—7, temperature—25°C, and agitation—100 rpm) on the adsorption of MG on Fe_3O_4@AJPAL.

high adsorbent dose [51, 52]. However, no significant increase in the adsorption efficiency above the 50 mg dose was observed. Moreover, the drop in the adsorption capacity is due to the aggregation events at a high dosage which lead to a decrease in the total surface area of the Fe_3O_4@JPL adsorbent. These outcomes are consistent with the results of the literature reported in [53]. As a result, under the examined condition, the optimal adsorbent dose was 50 mg.

3.2.5. Effect of Initial Concentration and Temperatures. The adsorption capacities of the Fe_3O_4@AJPL adsorbent at different initial MG concentrations (20–350 mg/L) and temperatures (25, 35, and 45°C) were also studied, keeping other factors (time: 120 min, pH: 7, dose: 50 mg, and agitation: 100 rpm) as given in Figure 5(d). The outcomes show that the adsorbed amount of MG dye by Fe_3O_4@AJPL was linearly increased while the initial MG concentration increased, e.g., as C_o was augmented from 20 to 350 mg/L, the adsorption capacity improved from 18.5 to 201.2 mg/g at 25°C. Such results can be ascribed to the increment in the driving force of the adsorbate concentration, resulting in a high diffusion rate of the MG dye from the liquid phase to the solid phase. At the higher C_o and at 45°C, the archived q_e value was 258.6 mg/g. Also, the adsorption capacity was increased from 18.5 to 20 mg/g with increasing temperature from 25°C to 45°C at 20 mg/L. This increase in adsorption capacity is possibly due to diffusion enhancement of MG molecules to the surface and pores of Fe_3O_4@AJPL which is driven by

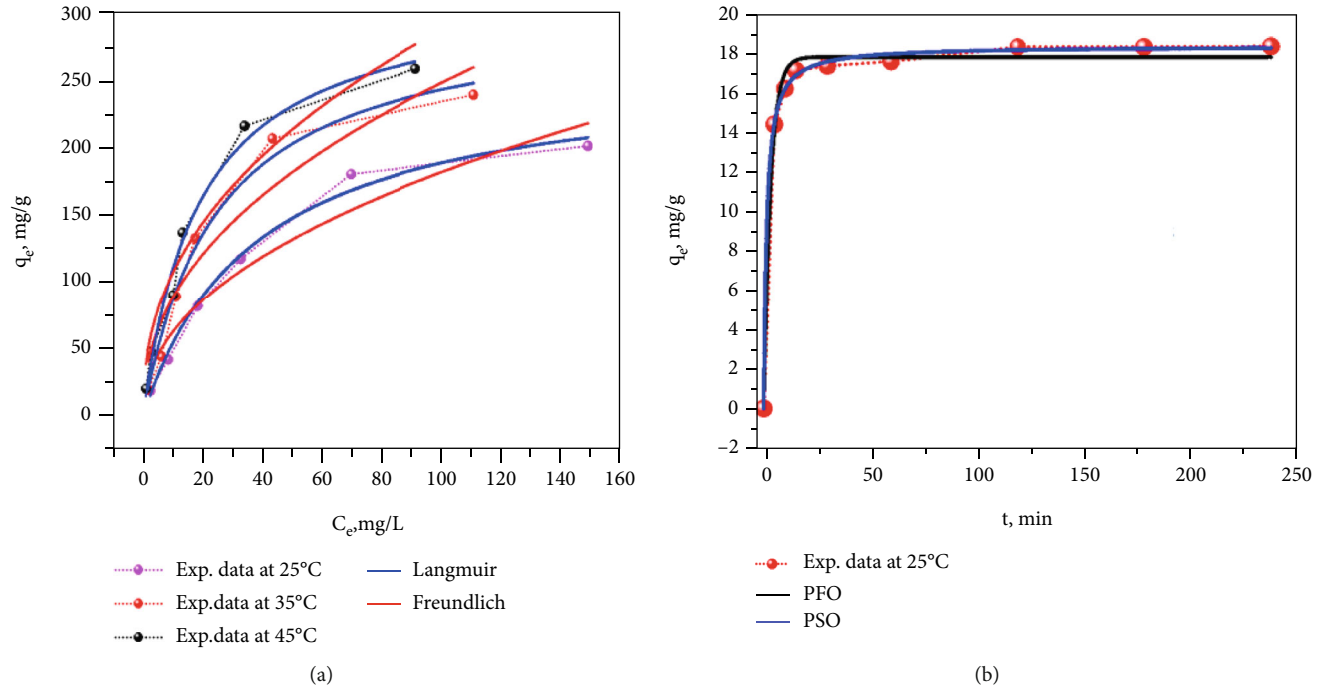

Figure 6: (a) Nonlinear adsorption isotherm at different temperature (conditions: MG—20-350 mg/L, time—120 min, Fe_3O_4@AJPAL—50 mg, pH—7, and agitation—100 rpm) and (b) nonlinear kinetic models for MG adsorption by Fe_3O_4@AJPAL (conditions: MG—20 mg/L, time—120 min, Fe_3O_4@AJPAL—50 mg, pH—7, temperature—25°C, and agitation—100 rpm).

Table 2: Langmuir and Freundlich isotherm models for MG adsorption on Fe_3O_4@AJPL nanocomposite (conditions: MG—20-350 mg/L, time—120 min, Fe_3O_4@AJPAL—50 mg, volume—0.05 L, and agitation—100 rpm).

Model	MG dye		
	298 K	308 K	318 K
Langmuir			
q_m (mg/g)	260.8	302.7	318.3
K_L (L/mg)	0.026	0.040	0.052
R_L	0.657	0.551	0.485
R^2	0.989	0.980	0.980
Freundlich			
K_f (mg/g) $(L/mg)^{1/n}$	21.67	31.65	39.91
R^2	0.929	0.894	0.925

elevated kinetic energy at higher temperature, thus suggesting an endothermic adsorption process. These outcomes are consistent with other studies for the removal of MG ions by organically modified clay [54] and Fe-Mg BACs [55].

3.3. Adsorption Modeling

3.3.1. Adsorption Isotherm. The adsorption isotherm studies were accomplished over a range of MG initial concentrations of 20–350 mg/L and at temperatures of 25, 35, and 45°C, keeping the other factors constants (i.e., adsorbent dose: 50 mg, pH: 7, contact time: 120 min, and agitation speed: 100 rpm). Nonlinear isotherm adsorption models such as Langmuir (Equation (4)) [56] and Freundlich (Equation (5)) [57] were applied to describe the behavior of the MG adsorption onto Fe_3O_4@AJPL.

$$q_e = \frac{q_m K_L C_e}{1 + K_L C_e}, \tag{4}$$

$$q_e = K_F C_e^{1/n}, \tag{5}$$

where q_m is the maximum adsorption capacity (mg/g), n is the adsorption intensity, K_F is the Freundlich isotherm constants, and K_L is the Langmuir constant. According to the isotherm data shown in Figure 6(a) and Table 2, it is clear that the Langmuir model ($R^2 = 0.989$) provided a better fit than the Freundlich one ($R^2 = 0.929$), suggesting monolayer coverage. The adsorbent capacity corresponding to the maximum monolayer coverage (q_m, mg/g) was 318.3 mg/g at 45°C. The separation factor (R_L) values during the work were found in favorable adsorption (<1) (i.e., 0.026, 0.040, and 0.052 at 298, 308, and 318 K). Moreover, the increase in the values of the K_F and K_L constants with temperature confirmed endothermic adsorption [58, 59].

3.3.2. Kinetic Adsorption. The adsorption mechanism was achieved using the nonlinear kinetic models and pseudo-first-order (PFO) and pseudo-second-order models described by the following equations:

$$q_t = q_e\left(1 - e^{-k_1 t}\right), \tag{6}$$

$$q_t = \frac{q_e^2 k_2 t}{1 + q_e k_2 t}, \tag{7}$$

Table 3: Kinetic model parameters for MG adsorption on Fe_3O_4@AJPL (conditions: MG—20 mg/L, time—120 min, Fe_3O_4@AJPAL—50 mg, volume—0.05 L, temperature—25°C, and agitation—100 rpm).

C_o (mg/L)	$q_{e,exp}$ (mg/g)	Pseudo-first-order			Pseudo-second-order		
		$q_{e1,cal}$ (mg/g)	K_1 (1/min)	R^2	$q_{e2,cal}$ (mg/g)	K_2 (g/mg-min)	R^2
20	18.35	17.80	0.308	0.991	18.36	0.040	0.998

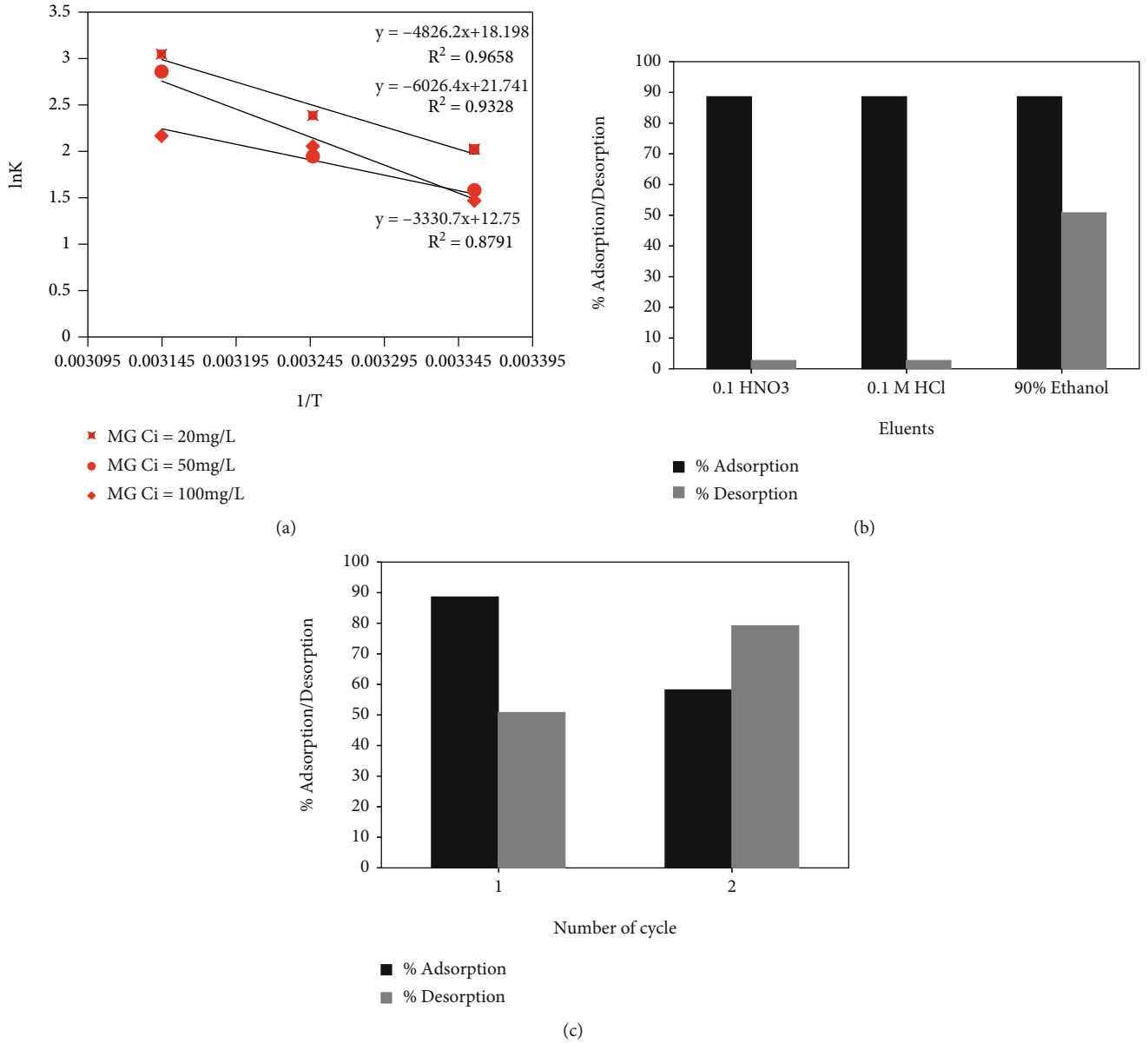

Figure 7: (a) Adsorption thermodynamics, (b) adsorption/desorption plot of MG dye from Fe_3O_4@AJPAL, and (c) recycling study (conditions: MG—20 mg/L, time—120 min, Fe_3O_4@AJPAL—50 mg, pH—7, temperature—25°C, and agitation—100 rpm).

where q_t (mg/g) is the adsorption capacity at time t (min) and k_1 and k_2 are the rate constants of PFO and PSO, respectively. Figure 6(b) displays the kinetic plots for the MG adsorption onto Fe_3O_4@AJPL. It was observed that adsorption was fast in the first stage of the adsorption period (20 min), then slowly developed until equilibrium (120 min). The calculated kinetic parameters are given in Table 3. On the basis of R^2 values, the adsorption kinetics fit PSO ($R^2 = 0.998$) better than the PFO ($R^2 = 0.991$), suggesting that the adsorption of MG onto Fe_3O_4@AJPL occurred by the chemisorption mechanism. Moreover, the q_e, calculated according to the PSO kinetic model ($q_{e,\,cal} = 18.36$ mg/g), was closer to the experimental

Table 4: Thermodynamic factors for adsorption of MG on Fe_3O_4@AJPL (conditions: time—120 min, Fe_3O_4@AJPAL—50 mg, volume—0.05 L, pH—7, and agitation—100 rpm).

Concentration MG dye	ΔH° (kJ/mol)	ΔS° (J/mol·K)	$(-)\Delta G^\circ$ (kJ/mol)		
			298 K	308 K	318 K
20	40.12	151.2	5.095	6.192	8.139
50	50.10	180.7	3.998	5.065	7.646
100	27.69	106.0	3.716	5.342	5.811

Table 5: Comparison of the MG adsorption capacity of Fe_3O_4@AJPL nanocomposite with other magnetic adsorbents.

Adsorbent	Conditions	q_m (mg/g)	Ref.
HNT-Fe_3O_4	C_o: 40-120 mg/L; T: 298 K; pH: 8; time: 240 min; dose: 150 mg	44.25	[49]
A litchi peel-based magnetic	C_o: 150 mg/L; pH: 6; T: 298 K; dose: 5.14 g/L; time: 66.69 min	70.42	[66]
PDA/CS/Fe_3O_4	C_o: 5-200 mg/L; T: 303 K; pH: 8; time: 40 min; dose: 100 mg	60.97	[67]
Magnetic pectin-Chlorella vulgaris	C_o: 5-100 mg/L; T: 303 K; dose: 50 mg; time: 30 min	247.2	[68]
3-MPA@PMNPs	C_o: 25 mg/L; T: 298 K; pH: 6; time: 120 min; dose: 500 mg	81.2	[69]
Fe_3O_4@AMCA-MIL-53 (Al)	C_o: 25-400 mg/L; T: 298 K; pH: 6.8; time: 210 min; dose: 20 mg	262.52	[70]
Fe_3O_4@AJPL	C_o: 25-350 mg/L; T: 318 K; pH: 7; time: 120 min; dose: 50 mg	318.3	This study

value ($q_{e,\,exp}$ = 18.35 mg/g), supporting the PSO model. Similar trends have been reported by other adsorbents [60, 61].

3.3.3. Adsorption Thermodynamics. The adsorption thermodynamic factors such as the Gibbs free energy (ΔG°), entropy (ΔS°), and enthalpy (ΔH°) for the removal of the MG dye onto the Fe_3O_4@AJPL nanocomposite were calculated using Equation (8) and the van't Hoff equation (Equation (9)) [62]:

$$\Delta G^\circ = -RT\ \ln K_c, \tag{8}$$

$$\ln K_c = -\frac{\Delta H^0}{RT} + \frac{\Delta S^0}{R}, \tag{9}$$

where R is gas constant (8.314 J/mol·K) and K_c represents the equilibrium constant and its equal q_e/c_e [63]; the other notations have the same meaning as above.

Figure 7(a) and Table 4 summarize the data obtained. The value of ΔG° obtained was negative, indicating that the adsorption of MG onto Fe_3O_4@AJPL is spontaneous. The positive values of ΔH° and ΔS° indicate the endothermic process and increase in randomness during the adsorption process, respectively. The temperature-dependent ΔG° revealed favorable adsorption at higher temperature; however, the effect of the initial concentration of MG suggests better adsorption at a lower concentration. Additionally, the value of $\Delta H^\circ > 40\ \text{kJ mol}^{-1}$ at a low concentration means that the mechanism of MG adsorption is chemisorption. Therefore, at the examined adsorption conditions, the obtained ΔG° and ΔH° values suggest physical and chemical adsorption mechanisms, respectively [64]. Similar trends have been reported by Arabkhani et al. for the removal of MG using the GO/MMT polymer nanocomposite [65].

3.4. Adsorption Mechanism. Figure 1 shows the stepwise preparation of the adsorbent Fe_3O_4@AJPL and the proposed adsorption mechanism. According to the FTIR spectrum, after MG dye adsorption on the Fe_3O_4@AJPL nanocomposite, there was a decrease and shift in the peak intensities of the functional groups. it was observed that the peaks at 3320 cm^{-1}, 1731 cm^{-1}, and 1026 cm^{-1} decrease and shift to 3329 cm^{-1}, 1721 cm^{-1}, and 1023 cm^{-1}, respectively, due to adsorptive interaction between the MG dye and the COOH, OH, and C-O-C groups on the Fe_3O_4@AJPL surface by different mechanisms such as hydrogen bonding, π-π stacking, and electrostatic interaction. The nonlinear isotherm and kinetic adsorption studies exhibited a better fit to PSO kinetic and Langmuir isotherm models, indicating chemisorption adsorption. Additionally, the weak desorption efficiency of MG from the Fe_3O_4@AJPL surface confirms the chemisorption mechanism. It was observed that adsorption of MG onto Fe_3O_4@AJPL was fast in the first stage of the adsorption period (15 min) then slowly developed until equilibrium (120 min). The initial rapid rate may indicate existence of available active sites on the Fe_3O_4@AJPL surface. Furthermore, the data indicate that more than 85.7% of MG molecules were adsorbed in the first stage, supporting the chemical adsorption mechanism. However, the first stage cannot be recognized, and the slow rate in the second adsorption phase suggests a physical mechanism, which is possibly controlled by the diffusion process. On the other hand, the thermodynamic data support the physisorption mechanism. Therefore, it could be concluded that the MG adsorption on Fe_3O_4@AJPL occurred by physical adsorption together with the chemisorption process. The EDX analysis clearly shows a new peak of nitrogen along with the peaks of elements of the Fe_3O_4@AJPL nanocomposite, indicating MG adsorption onto the whole surface of the Fe_3O_4@AJPL adsorbent.

3.5. Comparative Performance of Fe_3O_4@AJPL with Other Adsorbents. For comparative purposes, the maximum

adsorption capacity, q_m, of some other adsorbents reported in the literature for the MG uptake are given in Table 5 [49, 66–70]; the adsorption conditions are also tabulated for easy comparison. Obviously, the q_m value of Fe_3O_4@AJPL (318.3 mg/g) for MG adsorption is greater than the other listed magnetic nanocomposite adsorbents. The difference in the efficiencies of various adsorbents is due to the diversity in the adsorbent's structures and morphologies. Hence, the characteristics and performance of the investigated adsorbent, Fe_3O_4@AJPL, support its being appropriate as a potential adsorbent for the removal of cationic pollutants such as MG from polluted aqueous systems.

3.6. Desorption and Reusability Studies. To recover the MG dye from the Fe_3O_4@AJPL nanocomposite, three eluents, 0.1 M HCl, 0.1 M HNO_3, and ethanol (90%), were used (Figure 7(b)). From the results, it was observed that the recovery performance of ethanol was the highest (50.77%), while the acidic eluents (HCl and HNO_3) used showed only negligible efficiencies toward MG elution. The low recovery efficiency of MG from the Fe_3O_4@AJPL nanocomposite surface using ethanol indicates that most of the MG adsorption was probably by chemisorption. The outcomes of the kinetic and isotherm adsorption confirm the chemical adsorption mechanisms. The regeneration efficiency after two cycles was also examined. The result revealed that the adsorption efficiency of the MG dye on Fe_3O_4@AJPL was decreased from 89.5% to 58.2% as well as in the recovery percentage mostly due to incomplete desorption in the first cycle of the adsorption-desorption process as well as possible destruction of some active sites on the Fe_3O_4@AJPL surface.

4. Conclusion

In summary, a new magnetic nanocomposite (Fe_3O_4@AJPL) adsorbent was successfully synthesized via chemical activation of JPL and in situ coprecipitation with Fe_3O_4. The Fe_3O_4@AJPL nanocomposite was applied for the removal of the MG dye from aqueous solutions. The Fe_3O_4@AJPL nanocomposite was analyzed using different analytical techniques, and the results confirmed that the Fe_3O_4@AJPL nanocomposite was successfully synthesized. The surface area of the Fe_3O_4@AJPL nanocomposite was identified via BET analysis, and it is found to be 38.44 m^2/g. The Fe_3O_4@AJPL nanocomposite was tested to thoroughly clarify the influences of the factors on the adsorption of MG onto Fe_3O_4@AJPL. The optimized adsorption factors were found to be pH: 7, contact time: 120 min, adsorbent dose: 50 mg, temperature: 45°C, and initial MG concentration: 150 mg/L. The adsorption kinetic and isotherm were revealed to be a better fit to the PSO kinetic and Langmuir isotherm models. The maximum monolayer adsorption capacity was 318.3 mg/g at 45°C, which was greater than magnetic nanocomposite adsorbents reported previously. The thermodynamic studies indicated that the adsorption of MG onto Fe_3O_4@AJPL is a spontaneous and endothermic process. The interaction between the Fe_3O_4@AJPL nanocomposite and the MG dye occurred by chemisorption and physisorption that can be achieved by H-bonding, π–π interactions, and electrostatic attractions. The recovery results indicated that ethanol was the best eluent among the all the tested eluents. Overall, it could be concluded that the prepared Fe_3O_4@AJPL adsorbent will be a promising adsorbent for the elimination of MG dye from aqueous solutions

Data Availability

Anyone who wants to request research article data can contact me directly via the following email: aalorabi@bu.edu.sa, Chemistry Department, College of Science, Al Baha University.

Conflicts of Interest

There are no conflicts to declare.

Acknowledgments

We gratefully acknowledge the financial support by Albaha University (Project No. 1441/3) and are grateful to the Scientific Research Deanship.

References

[1] R. Bagheri, M. Ghaedi, A. Asfaram, E. Alipanahpour Dil, and H. Javadian, "RSM-CCD design of malachite green adsorption onto activated carbon with multimodal pore size distribution prepared from *Amygdalus scoparia*: Kinetic and isotherm studies," *Polyhedron*, vol. 171, pp. 464–472, 2019.

[2] F. Du, L. Sun, Z. Huang et al., "Electrospun reduced graphene oxide/TiO_2/poly(acrylonitrile- *co* -maleic acid) composite nanofibers for efficient adsorption and photocatalytic removal of malachite green and leucomalachite green," *Chemosphere*, vol. 239, article 124764, 2020.

[3] R. Gopinathan, J. Kanhere, and J. Banerjee, "Effect of malachite green toxicity on non target soil organisms," *Chemosphere*, vol. 120, pp. 637–644, 2015.

[4] A. A. Ahmad, M. A. Ahmad, N. K. E. M. Yahaya, and J. Karim, "Adsorption of malachite green by activated carbon derived from gasified *Hevea brasiliensis* root," *Arabian Journal of Chemistry*, vol. 14, no. 4, article 103104, 2021.

[5] H. Zhang, F. Zhang, and Q. Huang, "Highly effective removal of malachite green from aqueous solution by hydrochar derived from phycocyanin-extracted algal bloom residues through hydrothermal carbonization," *RSC Advances*, vol. 7, no. 10, pp. 5790–5799, 2017.

[6] M. Reza Shirzad Kebria and A. Rahimpour, "Membrane distillation: basics, advances, and applications," *Advances in Membrane Technologies*, vol. 67, 2020.

[7] S. P. Vinay, F. A. Alharthi, Udayabhanu, A. Alsalme, and G. Nagaraju, "Hydrothermal synthesis of Ag/rGO@CTFE nanocomposite as a promising photocatalyst for degradation action," *Journal of Molecular Structure*, vol. 1228, article 129722, 2021.

[8] B. Krishnakumar, A. Alsalme, F. A. Alharthi et al., "Synthesis, characterization of gelatin assisted ZnO and its effective

utilization of toxic azo dye degradation under direct sunlight," *Optical Materials*, vol. 113, article 110854, 2021.

[9] I. Oller, S. Malato, and J. A. Sánchez-Pérez, "Combination of Advanced Oxidation Processes and biological treatments for wastewater decontamination–A review," *Science of the Total Environment*, vol. 409, no. 20, pp. 4141–4166, 2011.

[10] C. A. Martínez-Huitle and E. Brillas, "Decontamination of wastewaters containing synthetic organic dyes by electrochemical methods: a general review," *Applied Catalysis B: Environmental*, vol. 87, no. 3-4, pp. 105–145, 2009.

[11] J. Labanda, J. Sabaté, and J. Llorens, "Modeling of the dynamic adsorption of an anionic dye through ion-exchange membrane adsorber," *Journal of Membrane Science*, vol. 340, no. 1-2, pp. 234–240, 2009.

[12] A. A. Alqadami, M. A. Khan, M. R. Siddiqui, and Z. A. Alothman, "Development of citric anhydride anchored mesoporous MOF through post synthesis modification to sequester potentially toxic lead (II) from water," *Microporous and Mesoporous Materials*, vol. 261, pp. 198–206, 2018.

[13] A. A. Alqadami, M. A. Khan, M. R. Siddiqui, Z. A. Alothman, and S. Sumbul, "A facile approach to develop industrial waste encapsulated cryogenic alginate beads to sequester toxic bivalent heavy metals," *Journal of King Saud University - Science*, vol. 32, no. 2, pp. 1444–1450, 2020.

[14] M. Alsuhybani, A. Alshahrani, M. Algamdi, A. A. Al-Kahtani, and A. A. Alqadami, "Highly efficient removal of Pb(II) from aqueous systems using a new nanocomposite: adsorption, isotherm, kinetic and mechanism studies," *Journal of Molecular Liquids*, vol. 301, article 112393, 2019.

[15] A. Q. Alorabi, M. Shamshi Hassan, and M. Azizi, "Fe_3O_4-CuO-activated carbon composite as an efficient adsorbent for bromophenol blue dye removal from aqueous solutions," *Arabian Journal of Chemistry*, vol. 13, no. 11, pp. 8080–8091, 2020.

[16] W. A. Amer, M. M. Omran, A. F. Rehab, and M. M. Ayad, "Acid green crystal-based *in situ* synthesis of polyaniline hollow nanotubes for the adsorption of anionic and cationic dyes," *RSC Advances*, vol. 8, no. 40, pp. 22536–22545, 2018.

[17] G. Crini, G. Torri, E. Lichtfouse, G. Z. Kyzas, L. D. Wilson, and N. Morin-Crini, "Dye removal by biosorption using cross-linked chitosan-based hydrogels," *Environmental Chemistry Letters*, vol. 17, no. 4, pp. 1645–1666, 2019.

[18] Ş. Parlayici, "Alginate-coated perlite beads for the efficient removal of methylene blue, malachite green, and methyl violet from aqueous solutions: kinetic, thermodynamic, and equilibrium studies," *Journal of Analytical Science and Technology*, vol. 10, no. 1, p. 4, 2019.

[19] R. Ben Arfi, S. Karoui, K. Mougin, and A. Ghorbal, "Adsorptive removal of cationic and anionic dyes from aqueous solution by utilizing almond shell as bioadsorbent," *Euro-Mediterranean Journal for Environmental Integration*, vol. 2, no. 1, pp. 1–13, 2017.

[20] B. H. Hameed and A. A. Ahmad, "Batch adsorption of methylene blue from aqueous solution by garlic peel, an agricultural waste biomass," *Journal of Hazardous Materials*, vol. 164, no. 2-3, pp. 870–875, 2009.

[21] L. S. Oliveira, A. S. Franca, T. M. Alves, and S. D. F. Rocha, "Evaluation of untreated coffee husks as potential biosorbents for treatment of dye contaminated waters," *Journal of Hazardous Materials*, vol. 155, no. 3, pp. 507–512, 2008.

[22] H. Tahir, M. Sultan, N. Akhtar, U. Hameed, and T. Abid, "Application of natural and modified sugar cane bagasse for the removal of dye from aqueous solution," *Journal of Saudi Chemical Society*, vol. 20, pp. S115–S121, 2016.

[23] A. A. Oyekanmi, A. Ahmad, K. Hossain, and M. Rafatullah, "Statistical optimization for adsorption of rhodamine B dye from aqueous solutions," *Journal of Molecular Liquids*, vol. 281, pp. 48–58, 2019.

[24] V. S. Munagapati, V. Yarramuthi, Y. Kim, K. M. Lee, and D.-S. Kim, "Removal of anionic dyes (reactive black 5 and Congo red) from aqueous solutions using banana peel powder as an adsorbent," *Ecotoxicology and Environmental Safety*, vol. 148, pp. 601–607, 2018.

[25] P. Janoš, H. Buchtová, and M. Rýznarová, "Sorption of dyes from aqueous solutions onto fly ash," *Water Research*, vol. 37, no. 20, pp. 4938–4944, 2003.

[26] O. Hamdaoui, F. Saoudi, M. Chiha, and E. Naffrechoux, "Sorption of malachite green by a novel sorbent, dead leaves of plane tree: equilibrium and kinetic modeling," *Chemical Engineering Journal*, vol. 143, no. 1-3, pp. 73–84, 2008.

[27] N. Gupta, A. K. Kushwaha, and M. C. Chattopadhyaya, "Adsorption studies of cationic dyes onto Ashoka (*Saraca asoca*) leaf powder," *Journal of the Taiwan Institute of Chemical Engineers*, vol. 43, no. 4, pp. 604–613, 2012.

[28] L. Bulgariu, L. B. Escudero, O. S. Bello et al., "The utilization of leaf-based adsorbents for dyes removal: a review," *Journal of Molecular Liquids*, vol. 276, pp. 728–747, 2019.

[29] H. S. al-Shehri, E. Almudaifer, A. Q. Alorabi, H. S. Alanazi, A. S. Alkorbi, and F. A. Alharthi, "Effective adsorption of crystal violet from aqueous solutions with effective adsorbent: equilibrium, mechanism studies and modeling analysis," *Environmental Pollutants and Bioavailability*, vol. 33, no. 1, pp. 214–226, 2021.

[30] M. D. Huff and J. W. Lee, "Biochar-surface oxygenation with hydrogen peroxide," *Journal of Environmental Management*, vol. 165, pp. 17–21, 2016.

[31] Y. Xue, B. Gao, Y. Yao et al., "Hydrogen peroxide modification enhances the ability of biochar (hydrochar) produced from hydrothermal carbonization of peanut hull to remove aqueous heavy metals: batch and column tests," *Chemical Engineering Journal*, vol. 200-202, pp. 673–680, 2012.

[32] A. A. Alqadami, M. Naushad, M. A. Abdalla, M. R. Khan, and Z. A. Alothman, "Adsorptive removal of toxic dye using Fe_3O_4 –TSC nanocomposite: equilibrium, kinetic, and thermodynamic studies," *Journal of Chemical & Engineering Data*, vol. 61, no. 11, pp. 3806–3813, 2016.

[33] M. Burits, K. Asres, and F. Bucar, "The antioxidant activity of the essential oils of Artemisia afra, Artemisia abyssinica and Juniperus procera," *Phytotherapy Research*, vol. 15, no. 2, pp. 103–108, 2001.

[34] M. Loizzo, R. Tundis, F. Conforti, A. Saab, G. Statti, and F. Menichini, "Comparative chemical composition, antioxidant and hypoglycaemic activities of *Juniperus oxycedrus* ssp. *oxycedrus* L. berry and wood oils from Lebanon," *Food Chemistry*, vol. 105, no. 2, pp. 572–578, 2007.

[35] B. Šarić-Kundalić, C. Dobeš, V. Klatte-Asselmeyer, and J. Saukel, "Ethnobotanical survey of traditionally used plants in human therapy of east, north and north-east Bosnia and Herzegovina," *Journal of Ethnopharmacology*, vol. 133, no. 3, pp. 1051–1076, 2011.

[36] M. Öztürk, İ. Tümen, A. Uğur, F. Aydoğmuş-Öztürk, and G. Topçu, "Evaluation of fruit extracts of six Turkish Juniperus species for their antioxidant, anticholinesterase and

antimicrobial activities," *Journal of the Science of Food and Agriculture*, vol. 91, no. 5, pp. 867–876, 2011.

[37] B. S. Ndazi, S. Karlsson, J. V. Tesha, and C. W. Nyahumwa, "Chemical and physical modifications of rice husks for use as composite panels," *Composites Part A: applied science and manufacturing*, vol. 38, no. 3, pp. 925–935, 2007.

[38] K. Le Van and T. T. Luong Thi, "Activated carbon derived from rice husk by NaOH activation and its application in supercapacitor," *Progress in Natural Science: Materials International*, vol. 24, no. 3, pp. 191–198, 2014.

[39] E. H. Ibrahim, M. Kilany, H. A. Ghramh, K. A. Khan, and S. ul Islam, "Cellular proliferation/cytotoxicity and antimicrobial potentials of green synthesized silver nanoparticles (AgNPs) using *Juniperus procera*," *Saudi Journal of Biological Sciences*, vol. 26, no. 7, pp. 1689–1694, 2019.

[40] A. A. Alqadami, M. A. Khan, M. Otero, M. R. Siddiqui, B.-H. Jeon, and K. M. Batoo, "A magnetic nanocomposite produced from camel bones for an efficient adsorption of toxic metals from water," *Journal of Cleaner Production*, vol. 178, pp. 293–304, 2018.

[41] M. A. Khan, A. A. Alqadami, M. Otero et al., "Heteroatom-doped magnetic hydrochar to remove post-transition and transition metals from water: synthesis, characterization, and adsorption studies," *Chemosphere*, vol. 218, pp. 1089–1099, 2019.

[42] A. Allafchian, Z. S. Mousavi, and S. S. Hosseini, "Application of cress seed musilage magnetic nanocomposites for removal of methylene blue dye from water," *International Journal of Biological Macromolecules*, vol. 136, pp. 199–208, 2019.

[43] Q. Tang, X. Tang, Z. Li et al., "Zn(II) removal with Activated *Firmiana Simplex* Leaf: kinetics and equilibrium studies," *Journal of Environmental Engineering*, vol. 138, no. 2, pp. 190–199, 2012.

[44] A. Alqadami, M. Naushad, M. A. Abdalla, T. Ahamad, Z. Abdullah Alothman, and S. M. Alshehri, "Synthesis and characterization of Fe_3O_4@TSC nanocomposite: highly efficient removal of toxic metal ions from aqueous medium," *RSC advances*, vol. 6, no. 27, pp. 22679–22689, 2016.

[45] G. Karthivashan, M. J. Masarudin, A. Umar Kura, F. Abas, and S. Fakurazi, "Optimization, formulation, and characterization of multiflavonoids-loaded flavanosome by bulk or sequential technique," *International Journal of Nanomedicine*, vol. 11, pp. 3417–3434, 2016.

[46] E. Ekmen, M. Bilici, E. Turan, U. Tamer, and A. Zengin, "Surface molecularly-imprinted magnetic nanoparticles coupled with SERS sensing platform for selective detection of malachite green," *Sensors and Actuators B: Chemical*, vol. 325, article 128787, 2020.

[47] A. Asfaram, M. Ghaedi, G. R. Ghezelbash et al., "Biosorption of malachite green by novel biosorbent *Yarrowia lipolytica isf7*: Application of response surface methodology," *Journal of Molecular Liquids*, vol. 214, pp. 249–258, 2016.

[48] X. Pan, G. Zuo, T. Su et al., "Polycarboxylic magnetic polydopamine sub-microspheres for effective adsorption of malachite green," *Colloids and Surfaces A: Physicochemical and Engineering Aspects*, vol. 560, pp. 106–113, 2019.

[49] C. De Marco, R. S. Mauler, T. S. Daitx et al., "Removal of malachite green dye from aqueous solutions by a magnetic adsorbent," *Separation Science and Technology*, vol. 55, no. 6, pp. 1089–1101, 2020.

[50] M. Gao, Z. Wang, C. Yang, J. Ning, Z. Zhou, and G. Li, "Novel magnetic graphene oxide decorated with persimmon tannins for efficient adsorption of malachite green from aqueous solutions," *Colloids and Surfaces A: Physicochemical and Engineering Aspects*, vol. 566, pp. 48–57, 2019.

[51] W. A. Amer, M. M. Omran, and M. M. Ayad, "Acid-free synthesis of polyaniline nanotubes for dual removal of organic dyes from aqueous solutions," *Colloids and Surfaces A: Physicochemical and Engineering Aspects*, vol. 562, pp. 203–212, 2019.

[52] M. Ghaedi, Z. Rozkhoosh, A. Asfaram, B. Mirtamizdoust, Z. Mahmoudi, and A. A. Bazrafshan, "Comparative studies on removal of erythrosine using ZnS and AgOH nanoparticles loaded on activated carbon as adsorbents: kinetic and isotherm studies of adsorption," *Spectrochimica Acta Part A: Molecular and Biomolecular Spectroscopy*, vol. 138, pp. 176–186, 2015.

[53] A. M. Aldawsari, I. H. Alsohaimi, A. A. Al-Kahtani, A. A. Alqadami, Z. E. Ali Abdalla, and E. A. M. Saleh, "Adsorptive performance of aminoterephthalic acid modified oxidized activated carbon for malachite green dye: mechanism, kinetic and thermodynamic studies," *Separation Science and Technology*, vol. 56, no. 5, pp. 835–846, 2021.

[54] S. Arellano-Cárdenas, S. López-Cortez, M. Cornejo-Mazón, and J. C. Mares-Gutiérrez, "Study of malachite green adsorption by organically modified clay using a batch method," *Applied Surface Science*, vol. 280, pp. 74–78, 2013.

[55] F. Guo, X. Jiang, X. Li, X. Jia, S. Liang, and L. Qian, "Synthesis of MgO/Fe_3O_4 nanoparticles embedded activated carbon from biomass for high-efficient adsorption of malachite green," *Materials Chemistry and Physics*, vol. 240, article 122240, 2020.

[56] A. Wallis and M. F. Dollard, "Local and global factors in work stress - the Australian dairy farming examplar," *Scandinavian Journal of Work, Environment and Health*, vol. 34, no. 6, pp. 66–74, 2008.

[57] H. Freundlich, *Über die adsorption in lösungen*, vol. 57, no. 1, 1907Zeitschrift Für Physikalische Chemie, 1907.

[58] S. Agarwal, I. Tyagi, V. K. Gupta, S. Mashhadi, and M. Ghasemi, "Kinetics and thermodynamics of malachite green dye removal from aqueous phase using iron nanoparticles loaded on ash," *Journal of Molecular Liquids*, vol. 223, pp. 1340–1347, 2016.

[59] S. N. Jain, Z. Shaikh, V. S. Mane et al., "Nonlinear regression approach for acid dye remediation using activated adsorbent: kinetic, isotherm, thermodynamic and reusability studies," *Microchemical Journal*, vol. 148, pp. 605–615, 2019.

[60] H. Jayasantha Kumari, P. Krishnamoorthy, T. K. Arumugam, S. Radhakrishnan, and D. Vasudevan, "An efficient removal of crystal violet dye from waste water by adsorption onto TLAC/chitosan composite: a novel low cost adsorbent," *International Journal of Biological Macromolecules*, vol. 96, pp. 324–333, 2017.

[61] P. Arabkhani, H. Javadian, A. Asfaram, and M. Ateia, "Decorating graphene oxide with zeolitic imidazolate framework (ZIF-8) and pseudo-boehmite offers ultra-high adsorption capacity of diclofenac in hospital effluents," *Chemosphere*, vol. 271, article 129610, 2021.

[62] A. A. Alghamdi, A.-B. Al-Odayni, W. S. Saeed et al., "Adsorption of azo dye methyl orange from aqueous solutions using alkali-activated polypyrrole-based graphene oxide," *Molecules*, vol. 24, no. 20, p. 3685, 2019.

[63] M. M. Ayad, W. A. Amer, S. Zaghlol, I. M. Minisy, P. Bober, and J. Stejskal, "Polypyrrole-coated cotton textile as adsorbent of methylene blue dye," *Chemical Papers*, vol. 72, no. 7, pp. 1605–1618, 2018.

[64] A. A. Alghamdi, A.-B. Al-Odayni, N. A. Y. Abduh, S. A. Alramadhan, M. T. Aljboar, and W. S. Saeed, "Adsorptive performance of polypyrrole-based KOH-activated carbon for the cationic dye crystal violet: kinetic and equilibrium studies," *Adsorption Science and Technology*, vol. 2021, article 5527594, pp. 1–11, 2021.

[65] P. Arabkhani, A. Asfaram, and M. Ateia, "Easy-to-prepare graphene oxide/sodium montmorillonite polymer nanocomposite with enhanced adsorption performance," *Journal of Water Process Engineering*, vol. 38, article 101651, 2020.

[66] H. Zheng, J. Qi, R. Jiang, Y. Gao, and X. Li, "Adsorption of malachite green by magnetic litchi pericarps: a response surface methodology investigation," *Journal of Environmental Management*, vol. 162, pp. 232–239, 2015.

[67] Y. Wang, Y. Zhang, C. Hou, and M. Liu, "Mussel-inspired synthesis of magnetic polydopamine-chitosan nanoparticles as biosorbent for dyes and metals removal," *Journal of the Taiwan Institute of Chemical Engineers*, vol. 61, pp. 292–298, 2016.

[68] A. C. Khorasani and S. A. Shojaosadati, "Magnetic pectin-*Chlorella vulgaris* biosorbent for the adsorption of dyes," *Journal of Environmental Chemical Engineering*, vol. 7, no. 3, article 103062, 2019.

[69] I. Ali, C. Peng, T. Ye, and I. Naz, "Sorption of cationic malachite green dye on phytogenic magnetic nanoparticles functionalized by 3-marcaptopropanic acid," *RSC Advances*, vol. 8, no. 16, pp. 8878–8897, 2018.

[70] A. A. Alqadami, M. Naushad, Z. A. Alothman, and T. Ahamad, "Adsorptive performance of MOF nanocomposite for methylene blue and malachite green dyes: kinetics, isotherm and mechanism," *Journal of Environmental Management*, vol. 223, pp. 29–36, 2018.